RESEARCH ARTICLE

NANO · MICRO small
www.small-journal.com

In-Situ Gas Permeation-Driven Ionic Current Rectification of Heterogeneously Charged Nanopore Arrays

*Sangjin Seo and Taesung Kim**

Ionic diodes provide ionic current rectification (ICR), which is useful for micro-/nanofluidic devices for ionic current-mediated applications. However, the modulation of ICR is not fully developed, and current challenges include limited active control and localized modulation for further multiplexing of micro-/nanofluidic ionic diodes. Herein, a microfluidic device integrated with particle-assembly-based ionic diodes (PAIDs) and a gas-flow channel above them is presented. Exploiting in-situ gas permeation through a polymeric film, precise control over the physiochemical conditions of the nanopores within the PAIDs, leading to the modulation of ICR is demonstrated. The investigation not only characterizes the rectification properties of the PAIDs but also unveils their capacitor-like behavior and the ability to actively modulate ICR using various gas flows. Furthermore, the reversible modulation of ICR through dynamic switching of gas-dissolved solutions, enabling ion-signal amplification is showcased. This pioneering approach of in situ gas-permeation offers programmable manipulation of ion transport along PAIDs, thereby positioning ionic diodes as versatile nanofluidic components. Looking ahead, the development of multiplexed PAIDs in an addressable manner on a chip holds promise for practical applications across diverse fields, including ion signaling, ion-based logic, chemical reactors, and (bio)chemical sensing.

1. Introduction

Nanoporous materials have been widely utilized to provide controlled ion transport based on nanoscale surface-dominated mechanisms.[1–4] Using ion-mediated mechanisms, the surface charge heterogeneity of nanopores achieves various functions, which are analogous to those of elementary electronic components.[5–9] Among them, ionic diodes have attracted considerable attention because of their ionic current rectification (ICR) functionality, where the directionality of ionic current can be controlled by the heterogeneously charged surfaces of nanopores.[10] Heterogeneous surface charges facilitate the asymmetric enhancement/blocking of ion transport within nanopores. These rectifying mechanisms have been studied experimentally and theoretically for mimicking the functions of biological membranes.[11,12] Moreover, the modulation of ICR based on chemical stimuli facilitates interesting applications. For example, ionic diodes were previously utilized for molecular detection by observing changes in the current or rectification behavior.[13,14] Protease detection and inhibitor screening were conducted using the logic operation of peptide-functionalized ionic diodes.[15] Moreover, stepwise asymmetrical modulation was achieved by the surface charges of nanochannel-based ionic pumps.[16,17] These applications demonstrated that a chemical stimulus can be used to control the surface charges of nanopores by adjusting the pH, ionic strength, and wettability,[18] as well as the presence of specific ions.[19]

Generally, facile methods for inducing sufficient chemical stimuli on submerged nanopores include complete replacement of the original solution with another solution of different pH[13,15,16,20] and generating acidic/basic gas bubbles in the solution.[21,22] As a result, changes in the chemical condition modify the surface charge of the nanopores from the exterior to the interior of the nanopores. Although existing methods reliably modulate ICR, the use of large volumes of solution is wasteful, and exchanging the liquid for simultaneous ion signal transduction is time-intensive. Moreover, bubble generation faces the same challenges of liquid exchange, along with miniaturization limitations. In addition to these challenges in active control, the lack of individual and localized control (i.e., addressability) limits the multiplexed working principle, which should be overcome with the versatility of micro-/nanofluidic devices.[23–25] In other words, if multiple ionic diodes share common liquid channels, the aforementioned methods cannot easily and individually apply chemical stimuli to each ionic diode.

S. Seo, T. Kim
Department of Mechanical Engineering
Ulsan National Institute of Science and Technology (UNIST)
50 UNIST-gil, Ulsan 44919, Republic of Korea
E-mail: tskim@unist.ac.kr

T. Kim
Department of Biomedical Engineering
Ulsan National Institute of Science and Technology (UNIST)
50 UNIST-gil, Ulsan 44919, Republic of Korea

The ORCID identification number(s) for the author(s) of this article can be found under https://doi.org/10.1002/smll.202402188

DOI: 10.1002/smll.202402188

As an alternative to direct handling of the aqueous solution, other stimuli were exploited to regulate the current asymmetricity of nanopores using light,[26] field effects,[27] or geometric deformation offering active ICR modulation.[28] Despite advancements in the controllability of microfluidic components, current methods still face challenges in regulating multiple ionic diodes separately on a chip. For instance, the light-meditated method of localized modulation requires an expensive light-exposure setup with a microscale exposure region. Precise alignment of the light sources is required to avoid interference between the multiple light sources, enabling independent operation of each ionic diode. The field-effect-mediated method is limited to silicon-based devices, which require sophisticated fabrication processes and prohibit optical observation. The geometric-deformation method—exemplified by bending or stretching—results in the modulation of multiple ionic diodes at the same time unless the local strain within a single device can be effectively discerned and utilized.[29] In this context, a method enabling addressability was developed in a previous study, where the ion-mediated neutralization of a hydrogel was used to modulate the ICR of hydrogel-based ionic diodes.[30] An ionic solution was manually injected into an open hole at the junction of the ionic diode to disable ICR, thereby releasing the amplified ionic signal. It seems possible to control multiple ionic diodes by selectively injecting ionic solutions into target ionic diodes. However, the ICR modulation was temporary as the ions in the injected solutions were consumed and dispersed. Moreover, to further broaden the practical applicability of ionic diodes and fully exploit the benefits of micro-/nanofluidic ionic diodes, additional advances must be achieved. An alternative can be the in situ delivery of stimulus molecules in an addressable manner to overcome the aforementioned limitations of conventional methods while minimizing effort for controlling multiplexed micro-/nanofluidic components.

In this study, we developed microfluidic devices with heterogeneous junctions fabricated using particle-assembled membranes (PAMs). Within multiple bridge microchannels, positive, and negative PAMs were fabricated in series, which serve as nanofluidic particle-assembly-based ionic diodes (PAIDs). A single microchannel was placed on top of ionic diodes, separated by a gas-permeable film that provides an in situ pathway for gas molecules to diffuse from the top microchannel toward the junction of the PAIDs in the bottom layer.[31] As a result, gas permeation can be induced via a solution-diffusion mechanism, causing a minimal but sufficient change in the physiochemical conditions within the PAIDs.[32] We characterized the properties of the PAIDs comprising chemically responsive particles in terms of their ICR and capacitor-like response under various electrical and chemical conditions. Further, we investigated the modulation of ICR through the flow of gas-dissolved solutions, achieving reversible changes in ICR and facilitating direct ionic signal amplification. Our study also involved exploring optimization strategies to enhance PAID performance for practical applications. Lastly, the developed PAIDs hold promise for various practical applications in micro-/nanofluidic systems although challenges such as further optimization and scalability need to be addressed in future research endeavors.

2. Result

Figure 1a shows a schematic of the developed microfluidic device comprising a main channel layer at the bottom, a control channel layer at the top, and a gas-permeable film separating the top and bottom layers. The bottom layer contains two parallel main channels, which are connected perpendicularly with ten bridge channels (length, $2L$ = 1 mm), through which ions flow under an electrical bias. Bridge channels with and without PAIDs were fabricated for comparison. The control channel serves as a gas-conditioning channel by flowing gas or gas-dissolved solutions; therefore, it was used not only to fabricate PAIDs but also to control gas permeation through the film. Additional details related to the fabrication process and dimensions of the microfluidic device are presented in Figure S1 and Note S1 (Supporting Information), respectively. Figure 1b shows the bridge channels connecting the two main channels that were used to form the PAIDs. The PAMs comprise nanopore networks, and their properties are governed by the particle characteristics, specifically their surface functionalization. Furthermore, the nanopores within the PAMs have been utilized as not only nanofluidic membrane structures but also ionic diodes, particularly.[33,34] In general, 200 nm sulfate-functionalized polystyrene (sPS) particles (pKa < 3) possess negatively charged surfaces, whereas 200 nm amidine-functionalized polystyrene (aPS) particles (pKa = 10–11) have positively charged surfaces over a wide pH range (from acidic to neutral).[35]

Typically, the minimum pore size of a PAM is estimated to be ≈15% of the particle diameter;[36] for example, 200 nm particles form pores of ≈30 nm, which is comparable to the Debye length (λ_D) generated for a solution with 1 mM of ionic strength (λ_D = 9.6 nm). Consequently, anions function as either counter ions or co-ions within the nanopore networks of aPS and sPS PAMs, respectively, with cations exhibiting the opposite behavior. Solutions with a wide range of pH levels can be used owing to the chemical robustness of PS. Figure S2 (Supporting Information) shows detailed scanning electron microscopy (SEM) images of the developed PAIDs. Bipolar PAMs (i.e., PAIDs) were formed under a flow of nitrogen gas using pervaporation-induced flow; the detailed fabrication process is provided in Figure S3 (Supporting Information) and our previous study.[37] The gas molecules are transported through the control channel either in the gaseous state or dissolved in water. Subsequently, the partial pressure difference of gases across the gas-permeable film initiates gas permeation toward the PAIDs. Acidic and basic gases dissolve and partially or fully dissociate into water to produce ions. The dissolved gases or dissociated ions may react with existing molecules, affecting the physiochemical conditions within the PAIDs.[35,38] Consequently, in-situ gas permeation to the PAIDs enables the control of their surface-charge heterogeneity.

Figure 1c shows I–V curves measured across the PAIDs after loading HCl solutions with three different concentrations into the main channels. Under forward bias, the current curves exhibit high slopes (i.e., significant current changes with respect to the applied voltage), whereas under reverse bias, the current remains quite low, close to zero. The current magnitudes show distinct differences between forward and reverse bias, indicating that the PAIDs exhibit ICR behavior. To quantify the degree

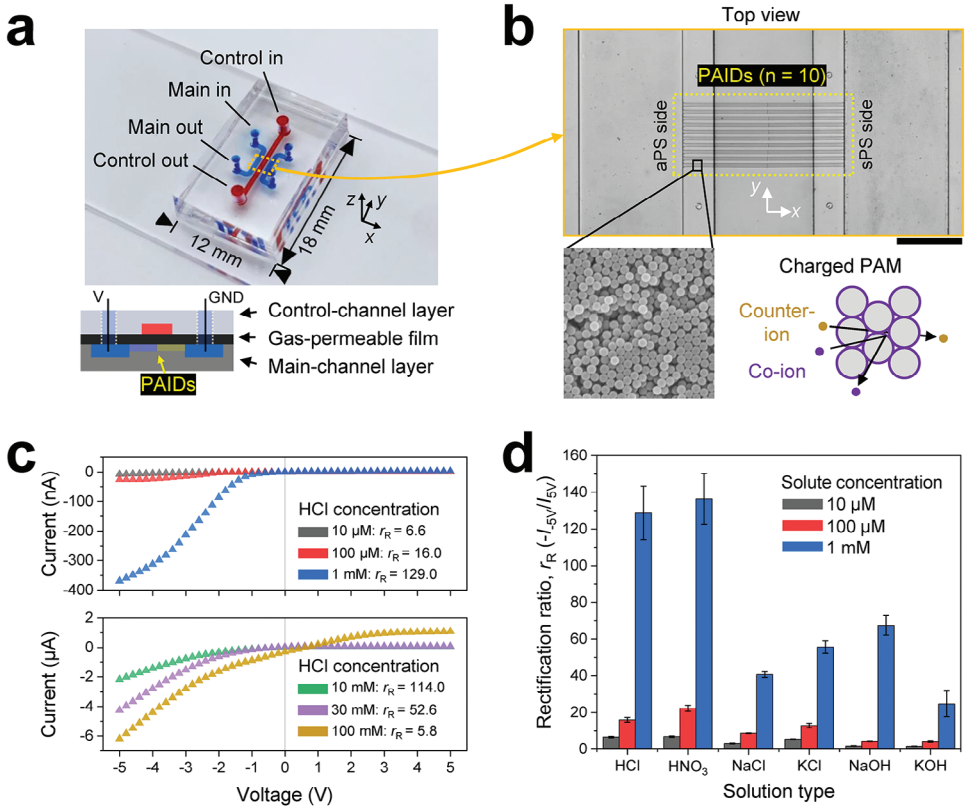

Figure 1. PAID-based microfluidic device and its working principles. a) Image of a microfluidic device filled with colored dyes to visualize the individual channel layers, as depicted in the cross-sectional view. b) Optical microscopy and SEM images of the bridge channels with the PAIDs. The pore network of the PAMs acts as a bundle of nanochannels with surface properties governed by the functionality of the particles. Black scale bar: 400 μm. c) *I–V* curves measured across PAIDs using various HCl solution concentrations. "Open" and "closed" states are observed in the forward bias (negative bias) and reverse bias (positive bias), respectively. Experiments were repeated three times, each using a single device for low (top) and high (bottom) concentration measurements. Error bars were omitted owing to their smaller size compared to the corresponding symbols. d) Rectification ratios ($-I_{-5\,V}/I_{5V}$) for various types and concentrations of solution in the main channel. Error bars represent the standard deviations of three measurements taken using an individual device for each type of solution to prevent contamination.

of ICR, we defined the rectification ratio as $r_R = -I_{-5\,V}/I_{5V}$, representing the ratio between the magnitudes of the current measured at −5 and +5 V. Within the low concentration range (10 μM–1 mM), the r_R increased with increasing magnitudes in forward currents owing to the variations of the solution conductivity, while magnitudes in reverse currents remained comparable. The zeta potential measurement (ζ) reveals that higher HCl concentrations lead to more positive values for both ζ_{aPS} and ζ_{sPS}, with the ζ_{sPS} eventually undergoing a sign switch beyond the 10 mM concentration threshold (Figure S4a, Supporting Information). The change of the ζ_{aPS} to a more positive value and the subsequent sign reversal of the ζ_{sPS} are influenced by pH, as the increased ionic strength of a monovalent solution typically leads to a decrease in the magnitude of zeta potentials.[39] Conversely, within the high concentration range (10–100 mM), the r_R decreased with increasing concentrations owing to the reduction in the charge heterogeneity of PAIDs and the decreasing λ_D. The gap between ζ_{aPS} and ζ_{sPS} gradually reduced with increasing concentrations, with a significant reduction observed above 30 mM. However, the decrease in the λ_D appeared to have a more pronounced effect on ICR, as evidenced by the steep decrease observed between 30 and 100 mM, despite a similar gap in zeta potentials. On the basis of the afore-described analysis of the ionic strength, we justified the use of lower concentrations, equal to or less than 1 mM, to maintain the ion-selectivity of PAMs while avoiding significant reduction in the λ_D.

Figure 1d shows the r_R of the PAIDs for various solution conditions in the main channels. The r_R values for all solution types exhibit increasing trends with increasing forward currents because of the solution conductivity; refer to Figure S5a (Supporting Information). The r_R values for acidic solutions (HCl and HNO_3) surpassed those for neutral solutions (NaCl and KCl) as well as basic solutions (NaOH and KOH). This significant difference in the r_R between the acidic and neutral solutions again originates from the disparity in conductivity. However, the forward currents and r_R values with basic solutions did not match the estimations calculated by interpolating the solution conductivities. In particular, the r_R values for basic solutions at the concentrations of 10 and 100 μM were significantly lower than those with other solutions. Figure S4b (Supporting Information) shows the reduction in the gap between ζ_{aPS} and ζ_{sPS}, along with a reversal in the sign of ζ_{aPS} induced by the presence of NaOH solution. This variation in charge heterogeneity leads to the loss of the ICR functionality and subsequent ion concentration polarization as confirmed

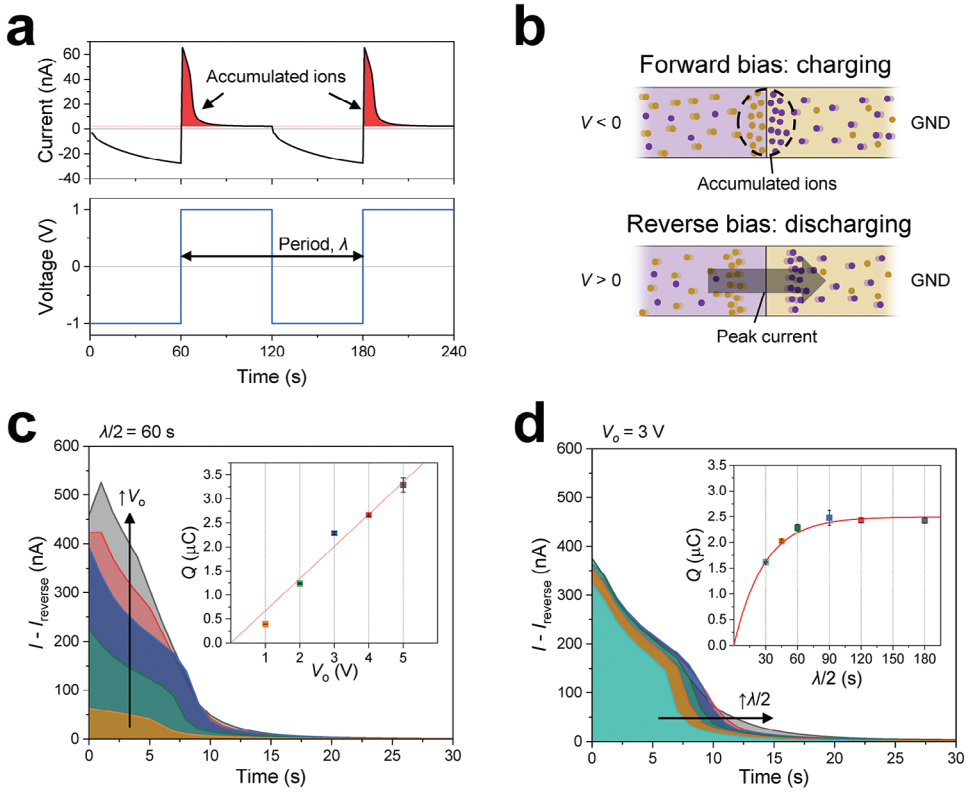

Figure 2. Capacitor-like properties of PAIDs. a) Transient current curves measured during the switching between forward bias (charging) and reverse bias (discharging). Switching biases, V_o, in both directions, were alternately applied with a period of λ. b) Schematic description of the charging and discharging processes under bias. Purple and yellow regions indicate positively and negatively charged PAMs, respectively. Purple and yellow dots indicate cations and anions, respectively. c) Discharging of ions with a fixed period but various switching biases. The accumulated charge (Q) has a linear relationship with V_o (inset). d) Discharging of ions with a fixed switching bias but various periods. Q has an asymptotic relationship with λ, similar to that of an electrolytic capacitor. Each curve in (c) and (d) represents the mean values of multiple experiments using a single device ($n = 6$), with the corresponding conditions marked in the insets using matching colors.

by distinct nonlinearities observed in forward bias (Figure S6, Supporting Information). These findings highlight the responsiveness of PAIDs to physiochemical conditions in terms of r_R. Furthermore, PAIDs experience a partial loss of their ICR functionality when exposed to basic solutions, indicating the potential for physiochemical stimuli-responsive modulation of ICR. Specifically, the forward current underwent significant changes in magnitude compared to the limited changes in reverse current (Figure S5b, Supporting Information). However, from an alternative perspective, the relative modulation ratio in the reverse current can surpass that in the forward current if the magnitude of the reverse current being modulated is relatively small.

It is interesting to note that current suppression was observed exclusively for PAIDs with $L = 500$ μm, while shorter PAIDs exhibited a linear behavior even under the same low-voltage conditions (see Figure S7a, Supporting Information). Such suppressions occurred within the voltage range of 0 to −1 V, regardless of solution types, although the degree of suppression appeared to vary with concentration (see Figure S6, Supporting Information). Moreover, the extent of suppression could be extended or reduced according to the scan rate (Figure S7b, Supporting Information). Prolonged measurement times with slower scan rates could induce a higher degree of ion accumulation within PAIDs, leading to nonlinearity at high voltages. Consequently, suppression demonstrated dependence on both PAID length and scan rate, indicating nonlinearity resulting from transient ion variations within PAIDs. Furthermore, current overshoots in the I–V curves were observed depending on the scanning direction (Figure S8, Supporting Information).[40] Hysteresis was observed after changes in the bias direction during scanning. In contrast to the decreasing bias scan (+5 to −5 V), during the increasing bias scan (−5 to +5 V), ion accumulation leads to current overshoot as the accumulated ions overflow from the PAIDs. These explorations of the hysteresis behaviors improve our understanding of the capacitor-like behavior of PAIDs, as discussed below.

Figure 2 describes the accumulation of ions within the PAIDs, highlighting their capacitor-like performance and providing a description of the associated parameters. Figure 2a shows the results of transient current measurements under repeated bias switching to demonstrate the accumulation of ions within the PAIDs. A switching bias of $V_o = 1$ V was applied while periodically changing the direction of the bias in a stepwise manner with a switching period of $\lambda = 120$ s. At the moment of switching to forward bias, the current was at its minimum, which is attributed to the depletion of ions within the PAIDs under reverse bias. However, the replenishment of ions restores the conductance, resulting in a progressive increase in the current over time (i.e., charging). After charging, switching to reverse bias

increases the maximum current values, which even surpasses the forward bias current. These current peaks arise from the sudden migration of accumulated ions out of the PAIDs (i.e., discharging). Subsequently, the current sharply declines shortly after the transition and converges to the leakage current values, indicating the re-depletion of the PAIDs. Schematics of these charging and discharging processes are presented in Figure 2b. The transient current with switching biases exhibits a hysteresis pattern similar to that shown in the *I–V* curve in Figure S8 (Supporting Information) but on a larger scale. Over time, current suppression diminishes as the PAIDs are refilled and accumulate ions. Abrupt switching to reverse bias induces current overshoot, albeit with a significantly higher magnitude.

Figure 2c shows the results of transient current measurements at the early stage of switching from forward to reverse bias with $\lambda = 120$ s, with various applied biases ranging from 1 to 5 V. The magnitude of the maximum current increases with increasing applied V_o. The total charge (Q) was evaluated by integrating the area under the current peak (see Note S2, Supporting Information). In the inset of Figure 2c and Q is plotted with respect to the applied and shows a linear dependence on voltage, parallel to the charging process of an electronic capacitor ($Q \propto V_o$). Figure 2d presents additional current measurement results at a fixed V_o of 3 V but under varying λ from 60 to 360 s. During evaluations, Q did not proportionally increase with increasing λ. Instead, the curves exhibited asymptotic saturation, mirroring the behavior of an electrolytic capacitor. The capacitor-like properties of PAIDs were well modeled with the primary parameters analogous to an electrolytic capacitor (see the inset of Figure 2d). All curves fit well with the equation describing the capacitor charging process (i.e., $Q(t) = CV_o[1 - e^{-t/\tau}]$), where C and τ represent the capacitance and time constant, respectively. The charging time (t) corresponds to half the period. Fitting the experimental data gave $C = 0.83$ μF and $\tau = 28.4$ s. The areal capacitance, considering the unit area as the minimum square containing PAIDs, was calculated to be 218.42 μF cm^{-2}, similar to 290 μF cm^{-2} given in a previous report with organic electronics.[4] Further, the linear relationship between Q and V_o in Figure 2c and the calculated τ were used as an alternative approach to calculate $C = 0.73$ μF, exhibiting a modest difference of 12.8% between the two distinct estimations. Consequently, the capacitance measured via calculating Q showed a simple relation with V_o and t, which will be helpful in predicting Q, e.g., for estimating an approximate number of target ions in detection applications.[34]

In this study, we assume that the response of the PAIDs to gas permeation varies depending on Q. This motivated our investigation of reverse bias conditions applied to the PAIDs during the gas-permeation experiments (corresponding to the results shown in **Figures 3** and 4), which aimed to continuously deplete ions and reduce the complexity associated with the transient state. Otherwise, experiments must consider the presence of remaining ions, as they can lead to hysteresis in current measurements and undesired reactions with permeating gases. Finally, our utilization of the capacitor-like behaviors was further developed for the fabrication of in situ ionic diodes, which is proposed in the Discussion Section.

Figure 3a shows the transient current across the bridge channels in the absence of PAIDs during the periodic switching of CO_2 flow (between on/off modes), i.e., a 60 s gas flow followed by a 30 min recovery phase, as shown in the inset. The automated experimental setup is presented in Figure S9 (Supporting Information). The measurements were conducted under a 1 V bias with a 1 mM KCl solution, and there was no reaction between the solute and the permeated CO_2 gas. The gas switching resulted in current peaks, reflecting the temporary increase in the bridge channel conductance due to CO_2 dissociation (see Note S3, Supporting Information), followed by a subsequent decrease in conductance during the recovery phase. The dispersion of CO_2 molecules in the absence of the PAIDs seems to promote slow recovery, leading to current drift over time (Figure S10, Supporting Information). After the gas flow was completely stopped to lower the conductance back to the initial value, the last measured values were taken as the baseline current (I_{base}) and used to calculate the current ($I-I_{base}$) for more accurate analysis and comparison of the data. Furthermore, the magnitude of the maximum currents, denoted with different-colored arrows in Figure 3a, altered periodically with the applied pressure (see Figure S11 and Note S4, Supporting Information). The linear relationship between maximum conductance and partial gas pressure was confirmed. As we expected, minimal stimuli on the most resistive component between the two electrodes dominantly affected the current signals. Furthermore, the slow but evident recovery implies the minimization of interference with the physiochemical condition of the main channels.

Figure 3b shows the transient currents measured using the PAIDs with a 1 mM HCl solution in the main channel and various reverse bias voltages (1–5 V) as N_2 and CO_2 gas was sequentially alternated with a switching interval of 5 min. The flow of CO_2 gas causes a greater increase in the current compared to that observed during the flow of N_2 gas, implying the permeation and dissociation of CO_2 gas despite the presence of the PAIDs. The current increase upon switching to N_2 gas is attributed to pervaporation-driven flow, which entails the withdrawal of ions from the main channels. Interestingly, the increments in the current are similar, regardless of the applied voltage, which conflicts with the intuitive expectation that the current increases proportionally with the voltage, considering the increase in the conductance of the PAIDs. To the best of our knowledge, this phenomenon arises from the rapid transport of ions induced by the applied bias, leading to an equilibrium within the PAIDs. In other words, the inflow of CO_2 seems to be balanced with the ions migrating toward the main channels (see Note S3, Supporting Information). Therefore, during the equilibrium state, the increase in current corresponds to the influx of CO_2 gas from the control channel.

Figure 3c shows similar current measurement results at a fixed reverse bias of 1 V with various solutions (i.e., HCl, KCl, and NaOH) introduced into the main channels. The permeation of CO_2 into the solutions with different solutions resulted in distinguishable differences in the transient currents. Rapid increases and decreases in the current were observed for the KCl and HCl solutions. In contrast, unlike the neutral KCl and acidic HCl solutions, the basic NaOH solution showed a similar steep increase in the current followed by a gradual increase upon introducing CO_2 gas. The steep increase was not as large as that observed for the other solutes because of a chemical reaction (see Note S5, Supporting Information). However, an ongoing reaction generated ion byproducts and increased the conductivity in the presence of

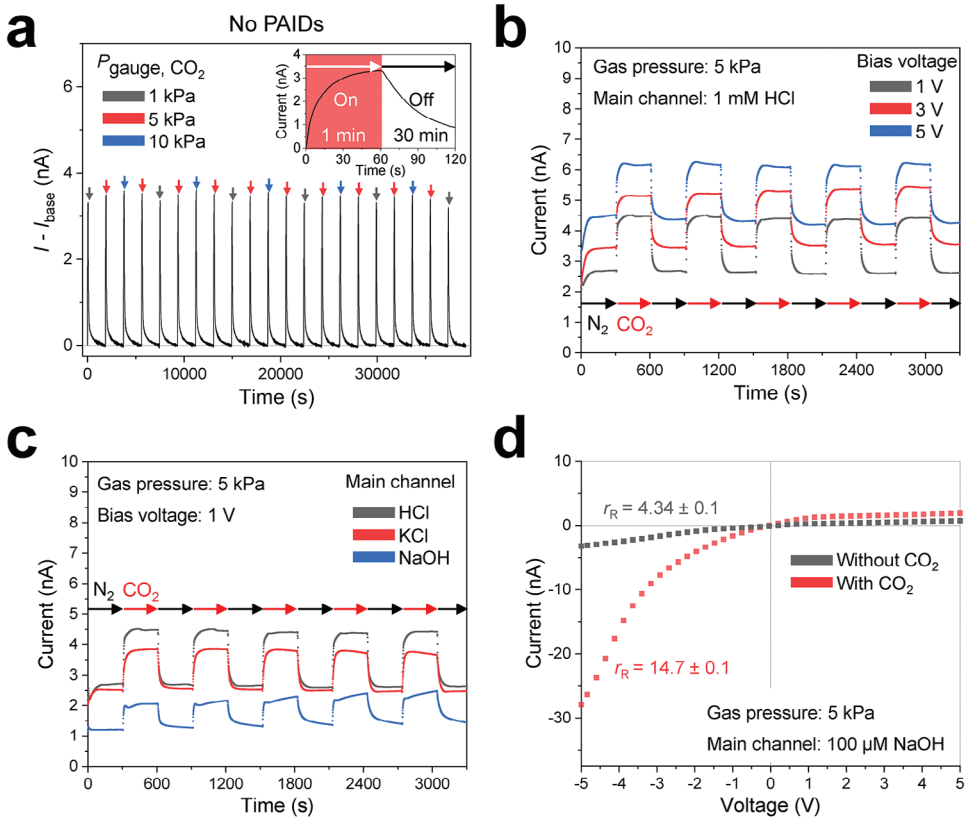

Figure 3. Currents measured using a gas-switching setup. a) Transient current curves were measured across the bridge channels without PAIDs. The flow of CO_2 gas in the control channel was repeatedly switched on and off. The CO_2 gas pressure was regulated to 1, 5, or 10 kPa. A magnified view of a current peak is shown in the inset. b) Transient current was measured across the PAIDs while the gas flow was repeatedly switched between N_2 and CO_2 (switching interval of 5 min). A 1 mM HCl solution was introduced into the main channels while various reverse biases were applied. c) Results of a similar experiment that introduced HCl, KCl, and NaOH solutions into the main channels while the bias was fixed at 1 V. d) *I–V* curves measured across PAIDs while a 100 μM NaOH solution was flowing in the main channels with/without CO_2 gas flow in the control channel. Currents were the average values of three measurements using a single device; the error bars were omitted because they were negligible.

OH^- ions, which are continuously available from the main channels. Furthermore, the recovery of the current after introducing N_2 gas exhibits a gradual drift, with an increasing trend observed throughout the entire measurement. This trend is attributed to the production of OH^- in the reverse reaction, impeding rapid recovery. The current responses during the periodic switching of gases indicate that gas permeation can indeed influence ionic transport within the PAIDs in a programmable manner. Specifically, the permeated gas induces self-dissociation and it further reacts with pre-existing molecules in the absence/presence of the PAIDs. Furthermore, the reactions may lead to significant changes in physiochemical conditions within the PAIDs compared to the case without any reaction.

Figure 3d shows the *I–V* curves of the PAIDs with 100 μM NaOH solutions in the absence/presence of CO_2 gas flow within the control channel. The pH neutralization of the basic solution was induced by CO_2 gas to manipulate the ICR of the PAIDs. In the absence of gas flow, the PAIDs exhibited a minimal r_R (4.34 ± 0.1). Subsequently, we introduced CO_2 gas and measured the *I–V* curves again using the same device. In contrast, a significant increase in the current magnitude was observed under forward bias compared to the previous experimental results. The pH decrease is attributed to the CO_2 gas flow that enhances r_R (14.7 ± 0.1). The solubility of pure CO_2 in deionized (DI) water at 298 K and 5 kPa is ≈35.7 mM (corresponding to a weak acid),[41] and only 123 μM of H^+ is generated under equilibrium, corresponding to a pH of 3.9. Moreover, the conductivity of DI water with dissolved CO_2 (48.5 μS cm^{-1}) is approximately double that of 100 μM NaOH (24.8 μS cm^{-1}). However, an approximately ninefold increase in the current was observed at −5 V under CO_2 gas flow, which indicates that the modulation of ICR is caused by the transition of the PAIDs from a basic state to either an acidic or neutral state. Through the above experiments, we controlled the physiochemical conditions of nanopores via in situ gas permeation through the PAIDs and eventually modulated ICR. However, the use of CO_2 provides poor reversible modulation of ICR, which is necessary for programmable modulation of ICR. The weakly acidic CO_2 gas remains undissociated in water during the *I–V* measurements, especially under forward bias. This undissociated CO_2 prohibits the PAIDs from recovering to their initial physiochemical state. To address this limitation, we further developed this method using a gas-dissolved solution. Most importantly, we were able to induce the permeation of both acidic and basic gases, achieving mutual neutralization.

Figure 4 shows an alternative approach for modulating the ICR with gas-dissolved solutions of HCl and NH_3 to mutually

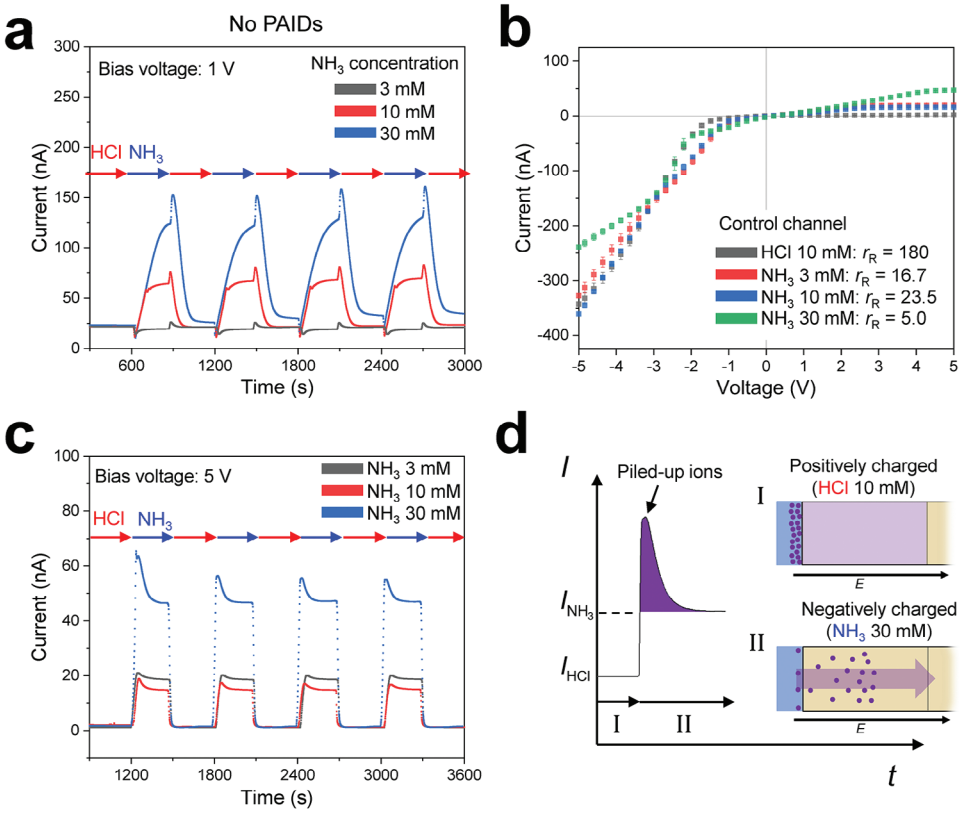

Figure 4. Currents measured during the switching of gas-dissolved solutions. a) Transient current measurement with 1 V across the bridge channels without PAIDs. HCl (10 mM) or NH_3 (3–30 mM) solutions were alternately flowed through the control channel and repeatedly switched every 5 min. b) *I–V* curves across PAIDs when various solutions were flowed through the control channel. Error bars represent the standard deviations of three measurements using a single device. c) Repetitive modulation of the PAIDs by switching the solutions in the control channel. Amplified peaks are observed at the time of neutralization (HCl→NH_3). d) Illustration describing the two-step ion-amplification mechanism: (phase I) H^+ ions accumulate as they are repelled from the positively charged membrane and (phase II) the accumulated ions are abruptly released at the time of the membrane neutralization by the NH_3 solution, resulting in peak currents that are larger than the saturated current values.

neutralize each other. Figure 4a shows the transient current measured across the bridge channels in the absence of the PAIDs when the gas-dissolved solutions in the control channel were switched between an HCl solution (fixed at 10 mM) and NH_3 solutions (3–30 mM) at a bias voltage of 1 V. Note that the main channel contained a 1 mM HCl solution throughout all of these experiments. An initial reduction in current was observed upon introducing the NH_3 solution, which is attributed to the neutralization reaction (see Note S6, Supporting Information). With NH_3 introduction, the current first decreases and then increases at the neutral point of the reaction. The maximum current, which was detected immediately after switching to the HCl solution, was attributed to the production of Cl^- and NH_4^+ owing to the reaction of the permeating HCl with the pre-existing NH_3 (a detailed explanation of the transient currents produced upon switching of the gas-dissolved solution is presented in Note S7, Supporting Information). Consequently, switching between gases with different acidities induces the neutralization of pre-existing H^+ and OH^- ions and gases. In addition, above the neutral points of pH, where permeating gas fully consumes pre-existing H^+ and OH^-, gases further permeate and dissociate into ions, resulting in a distinct chemical condition, particularly the pH, in a reversible manner. The gas permeation rate was directly regulated by the partial pressure/concentration of NH_3 in the solution, similar to the case using CO_2. To actively control these solutions, the experimental setup was amended as shown in Figure S12 (Supporting Information).

Figure 4b shows the *I–V* curves of PAIDs when the control channel was filled with gas-dissolved solutions of HCl and NH_3. These solutions enabled the reversible control of the physiochemical condition in PAIDs, facilitating programmable ICR modulation. The r_R is dependent on the type and concentration of the solutions and shows a broader range than that depicted in Figure 3d. The r_R decreases to 16.7 ± 0.1, 23.5 ± 0.3, and 5.0 ± 0.1 for the 3, 10, and 30 mM NH_3 solutions, respectively. Specifically, the PAIDs demonstrate notably increased reverse currents in the NH_3 solution (Figure S13, Supporting Information). In contrast, in a 10 mM HCl solution, the reverse current decreased significantly, even compared to the cases without gas flow, owing to the acidification of the PAIDs, leading to a high $r_R = 180 \pm 2.6$. These physiochemical responses of the PAIDs enabled ≈a 36-fold modulation of r_R, representing a considerably wider modulation range compared to the cases involving CO_2. The change in the reverse current with NH_3 solution appears to primarily originate from alterations in the surface charges of the aPS PAM (Figure S4b, Supporting Information). For aPS particles, zeta potentials

of 50.1 ± 0.8 mV and −52.8 ± 0.5 mV were measured in a 1 mM HCl (pH of 3) and a 30 mM NH_3 solution, respectively. These values are consistent with the general pH dependence of zeta potential values reported in the previous studies.[35,42] However, the zeta potential value of aPS in a 1 mM NaOH solution (pH ≈11) was negative but remained low (−16.7 ± 1.0 mV). The notable difference in magnitude is particularly unintuitive, given that the two solutions share similar pH levels. The similarity in pH also implies comparable ionic strengths, as pH reflects the degree of ionization. However, these alterations in zeta potential are not solely attributed to pH variations but are highly influenced by the unique property of the amidine-functional group.[43–46] The presence of excess NH_3 promotes amidine to function as an acidic group, resulting in both aPS and sPS PAM functioning as highly cation-selective pore networks rather than heterogeneously charged structures.

Consequently, NH_3 permeation attenuates the ICR functionality of the PAIDs and elevates the reverse current. In addition, the observed limiting currents under reverse bias with the NH_3 solution indicate ion concentration polarization. In fact, these limiting currents are similar to those observed when high concentrations (10–100 mM) of HCl solution in the main channel attenuated the ICR functionality of PAIDs, as depicted in Figure 1c. Importantly, unlike CO_2, the ion consumption by the neutralization reaction enables reversible modulation of ICR. Moreover, we compared two re-acidification methods for recovering the high r_R of the PAIDs by flowing DI water or 10 mM HCl solution through the control channel (Figure S14, Supporting Information). The permeation of HCl effectively recovers the *I*–*V* curves (with less hysteresis), whereas the use of DI water extended the voltage range of current suppression during repeated recovery tests. Both HCl and NH_3 gas facilitated the transition of the physiochemical condition of PAIDs to match that of the flowing gas by neutralizing the previous gas. Notably, the reversible changes in the reverse current indicate the possibility of an ionic gate. The permeation of gases into the PAIDs changed the reverse current from 1.77 to 47.38 nA at 5 V, corresponding to an on–off ratio of 26.8. Subsequently, ionic logic operations with gas stimuli have the potential to complement gate-voltage operations[5,47] by reducing the need for electric circuits enabling simple but still programmable actuation.

Figure 4c shows the transient currents measured across the PAIDs while the gas-dissolved solutions were periodically switched at a fixed reverse bias of 5 V. We first introduced a 10 mM HCl solution into the control channel, inducing ion depletion for 20 min, which resulted in a very low current. Second, we loaded NH_3 solutions for 5 min, resulting in a sharp increase in the current. Then, we repeatedly switched the solution in the control channel every 5 min. At the moment of switching from a well-rectifying state (HCl) to a poorly rectifying state (NH_3), maximum currents were generated, indicating amplified ionic signals. The maximum currents were followed by a plateau state with a magnitude dependent on the concentration of the NH_3 solution.

Figure 4d illustrates the mechanism underlying the generation of the current peak, which was proposed in a previous study.[30] The process involves the pile-up of ions at the entrance of the anion-selective PAIDs under reverse bias (phase I). Subsequently, the neutralization of PAIDs by gas-dissolved solutions triggers the abrupt release of the piled-up ions (phase II), generating the current peak. Therefore, current peaks are observed after each transition between HCl and NH_3, which were followed by asymptotic decreases in the current as the ions pass through the PAIDs. It is more reasonable that the current peaks originate from an ion-amplification process rather than a chemical reaction because they were not observed at the similar transition from HCl to NH_3 in Figure 4a. Furthermore, the increasing trend in the magnitude of gaps between the maximum current and the equilibrium current in phase II with increasing length of phase I is attributed to the amount of accumulated charge, rather than chemical reactions within the PAIDs; after a longer depletion process, more ions piled up at the entrance of the PAIDs and fewer ions remained accumulated within the PAIDs. Therefore, the ion-amplification process led to a current peak whereas chemical reactions led to gradual changes in the current over time (i.e., drift) for PAIDs under reverse bias (Figure 3c).

We quantified the accumulated charge by integrating the current ($I - I_{NH_3}$) over time (2 min) from the point where the current exceeded I_{NH_3} (i.e., $I > I_{NH_3}$) with the 30 mM NH_3 solution, giving values of 1.14, 0.54, 0.42, and 0.45 μC in the sequential order of the current peaks, where the first peak corresponds to the longest depletion time. The charge values obtained for the PAIDs at a bias of 5 V are 10–20 times smaller than that of the largest signal (≈12.5 μC) reported in the literature under similar conditions; specifically, the largest signal is reported using a hydrogel-based ionic diode of L = 450 μm with 100 mM KCl solution at a bias of 2 V.[30] This difference is attributed to the small cross-sectional area of the PAIDs, which was 18.5 times lower than the smallest cross-sectional area of ionic diodes reported in the literature. Benefitting from active controllability and reversibility, we confirmed that the switching between the "on" and "off" states is accomplished in ≈1 min. As indicated by the results, the responsiveness was fast enough to distinguish amplified signals from changing currents.

3. Discussion

The addressability and programmable modulation of ICR demonstrate the versatility of microfluidic ionic diodes. The combination of multiple PAIDs and control channels is considered beneficial for achieving a multiplexed actuation mechanism in a controllable manner, which is an important requirement of fully ionic logic gates. For example, the present device can be modified to contain homogeneous PAMs and multiple control channels, thereby enabling the switching between multiple types of junctions, such as p–n, n–p, n–p–n, and p–n–p components. Furthermore, there is ample room for improvement in amplifying the ionic current signal by optimizing the ICR. First, stronger electric fields can be generated by reducing the length of PAIDs. To compensate for the reduction in the length, modifications to the geometric and surface properties could be considered. For example, redesigning the bridge channels to achieve a conical shape could enhance current rectification.[10] Increasing the number of surface groups on the particles is expected to provide a broader range of surface-charge control. Second, the total cross-sectional area of the PAIDs could be significantly increased by fabricating densely packed bridge channels with larger cross-sectional areas. Incorporating control channels on multiple sides of the bridge channel could enhance the

gas permeation rate,[48] thereby facilitating the pervaporation-assisted assembly of particles in wider bridge channels. These optimization strategies should provide improved modulation of ICR and an increase in the height of the amplification peak.

Moreover, the hysteresis in ion transport is anticipated to be beneficial for applications utilizing ion accumulation. For example, the capacitor-like properties of p–n junctions, including their capacity and rate of accumulation, are crucial; similarly, ion accumulation within ionic diodes has recently attracted significant research attention.[34,49] Figure S15 (Supporting Information) demonstrates chemical reactions between accumulated ions and permeated gases, such as the neutralization reaction between accumulated H^+ ions and NH_3 molecules. The accumulated ions within ionic diodes are available for in situ chemical reactions, highlighting the potential for developing electrochemical sensors to detect target solutes or gases. Furthermore, adjusting the physiochemical conditions through gas permeation can enhance the fluorescent signal of accumulated target molecules, especially when pH sensitivity is crucial.

Future work on quantitative investigation is required to validate our experimental results and demonstrate practical applications. The development of suitable theoretical and numerical models is also essential. While we have proposed our most plausible explanation for the transient current during the switching of gas or gas-dissolved solution, a critical question remains on how surface charges of nanopores influence gas permeation and subsequent dissociations and reactions. To reduce the costs of numerical studies, the complexity of models arising from particle assembly and in situ gas permeation requires a perspective shift, e.g., by simplifying gas permeation in 3D nanoporous structures to a 2D condition in uniformly rectangular nanochannels. Understanding the role of the electric double layers in controlling the physiochemical conditions is the first step for anticipating simultaneous electrochemical phenomena with multiple species. The insights acquired from these studies are expected to guide the development and improvement of ion-signal amplification and molecular-sensing applications, allowing informed choices regarding the surface properties of nanopores, gas-permeable membranes, and microfluidic channel geometries.

4. Conclusion

We demonstrated the first modulation of ICR via in-situ gas permeation into ionic diodes. We fabricated heterogeneous junctions of PAMs as nanofluidic PAIDs with physiochemical responsivity and placed a polymeric membrane and a control channel above the PAIDs to facilitate in-situ gas permeation. When gases in the form of gas or gas-dissolved solution permeated into the aqueous solutions within PAID, the gases dissolved and sometimes further reacted with the aqueous solutions to modify the pH within the PAIDs. First, the dissociation and chemical reactions of permeating CO_2 gas were verified by observing differences in the current between various pre-existing solutions within PAIDs. Then, the PAIDs submerged in a basic aqueous solution showed an increase in ICR upon controlling the pH via CO_2 gas flow. Second, we demonstrated that gas-dissolved solutions enhanced the modulation of the r_R. The permeation of HCl and NH_3 gases led to the consumption of pre-existing H^+ or OH^-, resulting in the reversible control of the physiochemical condition within the PAIDs. Moreover, the dynamic alterations of the surface charge of the aPS particles induced by NH_3 resulted in a wide-range modulation of ICR (r_R = 5.0–180). Throughout the experiments, the switching of gases and gas-dissolved solutions was conducted using programmed systems, enabling active control of the PAIDs. Furthermore, the reversibility due to in situ acidification/alkalinization facilitates repeated switching of ICR, resulting in ion-signal amplification via processes based on the pile-up and abrupt release of ions. This finding further supports the potential of PAIDs for addressable modulation of the physiochemical condition within micro-/nanofluidic channels, in addition to that proposed in other literature.[37,41,50,51] In the future, additional numerical studies and optimization efforts to effectively combine ionic diodes with gas-permeation techniques are expected to provide a versatile nanofluidic platform for various applications. Furthermore, to realize active and multiplexed manipulation of multiple ionic diodes, we plan to investigate well-designed pairs of ionic diodes and control channels and develop a strategy to stabilize pH in the main channel using proper buffer solutions. Advances in the fabrication of 3D microfluidic devices also guarantee the development of multiplexed channel networks for addressable actuation.[52] We believe that the proposed gas manipulation method paves the way for deploying ionic diodes as versatile nanofluidic actuators for diverse applications, including ion signaling, ion-based logic, chemical reactors, and (bio)chemical sensing.

5. Experimental Section

Materials and Reagents: Photolithography was used to form primary molds for the control and main channel layers. Standard PDMS (Sylgard 184, Dow Corning, USA) and extra-hard PDMS (x-PDMS) were used to fabricate the control channel layer and gas-permeable film, respectively. x-PDMS was chosen for its high elastic modulus (≈80 MPa),[53] and thus its ability to resist film deformation under fluid flow pressure. All chemicals required for x-PDMS preparation, including linear vinyl siloxane (VDT-731), vinyl Q-siloxane (VQX-221), a moderator (SIT 7900.0), platinum catalyst (SIP 6831.2LC), and linear hydride siloxane (HMS-501) were procured from JSI Silicone, Korea. Ostemer resin (Ostemer 324 Flex, Mercene Labs, Sweden) was used for preparing a second mold. Another Ostemer resin (Ostemer 322 Clear, Mercene Labs) was used to fabricate the main channel layer. Ostemer 322 exhibits minimal gas permeability, which enhances the responsiveness of the main channels to the switching conditions induced by the control channel. Otherwise, the wall of the main channel acts as a reservoir for absorbing gas molecules under the gas-switching conditions. Chlorotrimethylsilane (92361, Merck, Germany) was used to enhance demolding. PAMs were fabricated using solutions of PS particles functionalized with sulfate (S37491, Thermo Fisher, USA) and amidine (A37314, Thermo Fisher), which are diluted to 0.5% with appropriate concentrations of aqueous KCl solutions. Pt electrodes (BASMW1032, Merck) were connected to the devices used for current measurements under various pH conditions. All ion solutes and solutions, including KCl, NaOH, HCl, and NH_3, were purchased from Merck.

Experimental Setup and Data Analysis: Optical and fluorescent images were captured using an inverted fluorescence microscope (Ti-E, Nikon, Japan) equipped with a charge-coupled device camera (ORCA R2; Hamamatsu Photonics, Japan). Bonding and silane treatment were performed using oxygen-plasma treatment (Cute-MP, Femto Science, Korea). A pressure-based gas-flow unit (MFCS-EZ, Fluigent, France) was used to introduce N_2 at a constant pressure during particle assembly. A gas

control unit comprising a solenoid valve array (S10MM-30-24-2, Pneumadyne Inc, USA), digital pressure regulators (ITV0010, SMC, Japan), and gas tanks were also used for switching gases or gas-dissolved solutions with precise pressure control. For automated switching, this unit was integrated with a control circuit controlled by an Arduino Mega R3 microcontroller (Adafruit Industries, USA) and corresponding Arduino codes. Current measurements were conducted using a sourcemeter (2600B, Keithley, USA). In general, the *I–V* curve measurements were performed at a scan rate of 20 mV s^{-1}, and the PAIDs remained stable. However, when utilizing basic solutions (NaOH or KOH), a scan rate of 40 mV s^{-1} was utilized to mitigate measurement deviation originating from structural instability. The instability becomes apparent in the measurement using 1 mM basic solutions, as observed by significant deviations in Figure S6e,f (Supporting Information), whereas moderate deviations were observed in lower concentrations. All zeta potential values were calculated using the Smoluchowski equation with the electrophoretic mobility obtained from a Zetasier Nano ZS system (Malvern Panalytical, UK). All values of zeta potential are quoted as the average ± standard deviation ($n = 3$). SEM images were obtained using a field emission scanning electron microscope (S-4800, Hitachi, Japan). ImageJ (National Institutes of Health, USA) and OriginPro 2020 software (OriginLab Corp., USA) were employed for image and data analysis, respectively.

Supporting Information

Supporting Information is available from the Wiley Online Library or from the author.

Acknowledgements

This work was supported by a National Research Foundation of Korea (NRF) grant funded by the Korean government (MSIT) (NRF-2020R1A2C3003344 and NRF-2020R1A4A2002728). All microfabrication processes were performed at the UNIST Central Research Facility Center.

Conflict of Interest

The authors declare no conflict of interest.

Author Contributions

S.S. and T.K. conceived this work. S.S. conducted all experiments and analyzed all data under the supervision of T.K. The authors contributed to writing and revising the manuscript.

Data Availability Statement

The data that support the findings of this study are available from the corresponding author upon reasonable request.

Keywords

gas permeation, ionic current rectification, ionic diode, micro-/nanofluidics, particle-assembly

Received: April 27, 2024
Revised: June 11, 2024
Published online:

[1] K. Xiao, C. Wan, L. Jiang, X. Chen, M. Antonietti, *Adv. Mater.* **2020**, *32*, 2000218.
[2] Y. Yan, J. Schiffbauer, G. Yossifon, H.-C. Chang, *J. Chem. Phys.* **2015**, *143*, 224705.
[3] C. H. Yang, B. Chen, J. J. Lu, J. H. Yang, J. Zhou, Y. M. Chen, Z. Suo, *Extreme Mechan. Lett.* **2015**, *3*, 59.
[4] P. Janson, E. O. Gabrielsson, K. J. Lee, M. Berggren, D. T. Simon, *Adv. Mater. Technol.* **2019**, *4*, 1800494.
[5] R. Karnik, R. Fan, M. Yue, D. Li, P. Yang, A. Majumdar, *Nano Lett.* **2005**, *5*, 943.
[6] K. Tybrandt, K. C. Larsson, A. Richter-Dahlfors, M. Berggren, *Proc. Natl. Acad. Sci. U.S.A.* **2010**, *107*, 9929.
[7] K. Tybrandt, E. O. Gabrielsson, M. Berggren, *J. Am. Chem. Soc.* **2011**, *133*, 10141.
[8] X. Wu, T. L. D. Tam, S. Chen, T. Salim, X. Zhao, Z. Zhou, M. Lin, J. Xu, Y. L. Loo, W. L. Leong, *Adv. Mater.* **2022**, *34*, 2206118.
[9] R. Karnik, C. Duan, K. Castelino, H. Daiguji, A. Majumdar, *Nano Lett.* **2007**, *7*, 547.
[10] X. Huang, X.-Y. Kong, L. Wen, L. Jiang, *Adv. Funct. Mater.* **2018**, *28*, 1801079.
[11] Z. S. Siwy, S. Howorka, *Chem. Soc. Rev.* **2010**, *39*, 1115.
[12] X. Kan, C. Wu, L. Wen, L. Jiang, *Small Methods* **2022**, *6*, 2101255.
[13] R. Peng, Y. Pan, B. Liu, Z. Li, P. Pan, S. Zhang, Z. Qin, A. R. Wheeler, X. S. Tang, X. Liu, *Small* **2021**, *17*, 2100383.
[14] G. Laucirica, Y. Toum Terrones, V. Cayón, M. L. Cortez, M. E. Toimil-Molares, C. Trautmann, W. Marmisollé, O. Azzaroni, *TrAC, Trends Anal. Chem.* **2021**, *144*, 116425.
[15] L. Shi, D. Kuang, X. Ma, M. Jalalah, S. A. Alsareii, T. Gao, F. A. Harraz, J. Yang, G. Li, *Nano Lett.* **2022**, *22*, 1083.
[16] H. Zhang, X. Hou, L. Zeng, F. Yang, L. Li, D. Yan, Y. Tian, L. Jiang, *J. Am. Chem. Soc.* **2013**, *135*, 16102.
[17] Z. Zhang, P. Li, X. Y. Kong, G. Xie, Y. Qian, Z. Wang, Y. Tian, L. Wen, L. Jiang, *J. Am. Chem. Soc.* **2018**, *140*, 1083.
[18] J. Zhang, Y. Yang, Z. Zhang, P. Wang, X. Wang, *Adv. Mater.* **2014**, *26*, 1071.
[19] G. Perez-Mitta, A. G. Albesa, W. Knoll, C. Trautmann, M. E. Toimil-Molares, O. Azzaroni, *Nanoscale* **2015**, *7*, 15594.
[20] I. Vlassiouk, T. R. Kozel, Z. S. Siwy, *J. Am. Chem. Soc.* **2009**, *131*, 8211.
[21] H. Jiang, E. Wang, J. Wang, *RSC Adv.* **2015**, *5*, 35622.
[22] Y. Xu, M. Zhang, T. Tian, Y. Shang, Z. Meng, J. Jiang, J. Zhai, Y. Wang, *NPG Asia Mater.* **2015**, *7*, e215.
[23] Y. Wang, Y. Gao, Y. Yin, Y. Pan, Y. Wang, Y. Song, *Mikrochim. Acta* **2022**, *189*, 139.
[24] Z. Liao, J. Wang, P. Zhang, Y. Zhang, Y. Miao, S. Gao, Y. Deng, L. Geng, *Biosens. Bioelectron.* **2018**, *121*, 272.
[25] N. Venugopal Menon, S. B. Lim, C. T. Lim, *Curr. Opin. Pharmacol.* **2019**, *48*, 155.
[26] J. Lu, Y. Jiang, T. Xiong, P. Yu, W. Jiang, L. Mao, *Anal. Chem.* **2022**, *94*, 4328.
[27] W. Guan, R. Fan, M. A. Reed, *Nat. Commun.* **2011**, *2*, 506.
[28] H.-R. Lee, J. Woo, S. H. Han, S.-M. Lim, S. Lim, Y.-W. Kang, W. J. Song, J.-M. Park, T. D. Chung, Y.-C. Joo, J.-Y. Sun, *Adv. Funct. Mater.* **2019**, *29*, 1806909.
[29] M. Li, S. Chen, B. Fan, B. Wu, X. Guo, *Adv. Funct. Mater.* **2020**, *30*, 2003214.
[30] S. M. Lim, H. Yoo, M. A. Oh, S. H. Han, H. R. Lee, T. D. Chung, Y. C. Joo, J. Y. Sun, *Proc. Natl. Acad. Sci. U.S.A.* **2019**, *116*, 13807.
[31] S. Seo, T. Kim, *Biomicrofluidics* **2023**, *17*, 061301.
[32] M. Polinkovsky, E. Gutierrez, A. Levchenko, A. Groisman, *Lab Chip* **2009**, *9*, 1073.
[33] T. Xiao, J. Ma, Z. Liu, B. Lu, J. Jiang, X. Nie, R. Luo, J. Jin, Q. Liu, W. Li, J. Zhai, *J. Mater. Chem. A* **2020**, *8*, 11275.

[34] J. Kim, J. Jeon, C. Wang, G. T. Chang, J. Park, *ACS Nano* **2022**, *16*, 8253.
[35] D. Herman, *Controlling Colloidal Stability Using Highly Charged Nanoparticles*, Virginia Polytechnic Institute and State University, VA **2015**.
[36] O. Schepelina, I. Zharov, *Langmuir* **2006**, *22*, 10523.
[37] S. Seo, J. Bae, H. Jeon, S. Lee, T. Kim, *Lab Chip* **2022**, *22*, 1474.
[38] K. N. Al-Milaji, V. Radhakrishnan, P. Kamerkar, H. Zhao, *J. Colloid Interface Sci.* **2018**, *529*, 234.
[39] B. J. Kirby, E. F. Hasselbrink Jr., *Electrophoresis* **2004**, *25*, 187.
[40] J. H. Han, K. B. Kim, J. H. Bae, B. J. Kim, C. M. Kang, H. C. Kim, T. D. Chung, *Small* **2011**, *7*, 2629.
[41] S. Shin, O. Shardt, P. B. Warren, H. A. Stone, *Nat. Commun.* **2017**, *8*, 15181.
[42] D. Herman, J. Y. Walz, *Langmuir* **2013**, *29*, 5982.
[43] E. F. Cornell, *J. Am. Chem. Soc.* **1928**, *50*, 3311.
[44] R. L. Shriner, F. W. Neumann, *Chem. Rev.* **1944**, *35*, 351.
[45] E. C. Franklin, *The Nitrogen System of Compounds*, Reinhold Publishing Corporation, New York **1935**.
[46] S. Soloveichik, H. Krakauer, *J. Chem. Educ.* **1966**, *43*, 532.
[47] J. Ji, M. Li, Z. Chen, H. Wang, X. Jiang, K. Zhuo, Y. Liu, X. Yang, Z. Gu, S. Sang, Y. Shu, *Nano Res.* **2019**, *12*, 1943.
[48] M. Dabaghi, N. Saraei, G. Fusch, N. Rochow, J. L. Brash, C. Fusch, P. R. Selvaganapathy, *J. Membr. Sci.* **2020**, *596*, 117741.
[49] S. H. Han, S. I. Kim, M. A. Oh, T. D. Chung, *Proc. Natl. Acad. Sci. U.S.A.* **2023**, *120*, 2211442120.
[50] S. Seo, D. Ha, T. Kim, *Nat. Commun.* **2021**, *12*, 1336.
[51] J. de Jong, P. W. Verheijden, R. G. Lammertink, M. Wessling, *Anal. Chem.* **2008**, *80*, 3190.
[52] J. Bae, R. Wu, T. Kim, *Small Methods* **2023**, 2300211.
[53] M. A. Verschuuren, *Substrate Conformal Imprint Lithography for Nanophotonics*, University Utrecht, The Netherlands **2010**.